Energy Storage Materials 88 (2026) 105063

Contents lists available at ScienceDirect

Energy Storage Materials

journal homepage: www.elsevier.com/locate/ensm

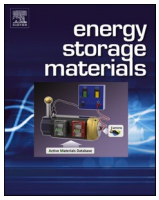

Engineering moderate solvation via molecular dipole modulation to guide robust interface for high-voltage Li metal batteries

Jiping Ma [a], Bo Zhang [a], Yang Gao [a], Lifeng Hou [a], Yinghui Wei [a,b], Shi Wang [c,d,*], Zhong Jin [c,*], Qian Wang [a,b,*]

[a] College of Materials Science and Engineering, Taiyuan University of Technology, Taiyuan, 030024, Shanxi, China
[b] Shanxi Key Laboratory of Corrosion and Control of Metal Materials, Taiyuan, 030024, Shanxi, China
[c] School of Chemistry and Chemical Engineering, Nanjing University, Nanjing, Jiangsu 210023, China
[d] State Key Laboratory of Organic Electronics & Information Displays (SKLOEID), Institute of Advanced Materials (IAM), Nanjing University of Posts & Telecommunications, Nanjing, 210023, China

ARTICLE INFO

Keywords:
Li metal batteries
High-voltage
Molecular dipole modulation
SEI film
Solvation

ABSTRACT

Conventional ether-based electrolytes, though favorable for uniform Li deposition, often undergo severe oxidative decomposition at high voltages, limiting their application in high-energy Li metal batteries (LMBs). Here, we propose a molecular dipole modulation strategy to enhance its high-voltage stability, wherein traditional ether-based 1,2-Dimethoxyethane (DME) molecules is redesigned into 3-ethoxylated propionitrile (EPN) through alkyl elongation and cyano-functionalization. Meanwhile, this structurally tailored solvent achieves a balanced charge dispersion and moderated solvation capability, which not only promotes the Li^+ de-solvation process but also actively guides the preferential decomposition of $DFOB^-$ anions toward forming a robust interphase rich in LiF and Li_3N, thereby effectively suppressing Li dendrite growth and side reactions on the cathode surface under high-voltage operation (via stable CEI film with ~5 nm). As a result, this well-designed electrolyte system demonstrates a high electrochemical window of 4.9 V, and corresponding Li||$LiFePO_4$ cells can run stably over 540 cycles at 1.0 C. More importantly, the high-voltage Li|| $LiNi_{0.7}Co_{0.1}Mn_{0.2}O_2$ (NCM712) cells can maintain a high coulombic efficiency (CE) of 99.9% over 300 cycles at 0.5 C, demonstrating remarkable stability under high-voltage conditions. This work demonstrates the importance of molecular dipole modulation for solvation structures and interface chemistry, offering an advanced electrolyte design paradigm for high-voltage LMBs.

1. Introduction

Nowadays, the rapid development of electric vehicles, aerospace and intelligent manufacturing has created an increasingly urgent demand for high-energy-density energy storage devices. Li metal anode, with a high theoretical capacity (3860 mAh g^{-1}) and the lowest electrochemical potential (3.04 V vs. SHE), endows LMBs with ultra-high energy density (>500 Wh kg^{-1}), standing out as a prime candidate for next-generation battery systems [1–3]. However, the practical application of LMBs is hindered by the incompatible requirements at the electrode-electrolyte interface. Specifically, the Li metal anode necessitates an electrolyte that enables uniform, dendrite-free Li deposition, while the high-voltage cathode demands exceptional oxidative stability [4]. Unfortunately, currently commercialized carbonate-based electrolytes exhibit poor compatibility with Li metal anode, often resulting in unstable solid electrolyte interface (SEI) film and rapid performance degradation, further limiting the cycling stability of LMBs [5,6].

By contrast, ether-based electrolytes, exemplified by 1,2-dimethoxyethane (DME), satisfy the former criterion due to their favorable Li^+ solvation energy, which promotes homogeneous Li plating [7–10]. However, their inherent low highest occupied molecular orbital (HOMO) energy level renders them susceptible to severe oxidative decomposition at potentials >4.0 V, leading to severe side reactions and rapid capacity fade and precluding their match with high-voltage cathodes [11–13]. This fundamental limitation creates a critical bottleneck for developing high-energy LMBs. To overcome this bottleneck, extensive efforts have been dedicated. Common strategies, such as introducing high-concentration salts or formulating localized

* Corresponding authors.
E-mail addresses: iamshiwang@njupt.edu.cn (S. Wang), zhongjin@nju.edu.cn (Z. Jin), qianwang0825@pku.edu.cn (Q. Wang).

https://doi.org/10.1016/j.ensm.2026.105063
Received 29 December 2025; Received in revised form 14 March 2026; Accepted 25 March 2026
Available online 26 March 2026

high-concentration electrolytes, often enhance stability at the expense of ionic conductivity, cost, and low-temperature performance [14–17]. Alternatively, the incorporation of film-forming additives can *in situ* generate a protective cathode electrolyte interphase (CEI) [18]. However, such approaches are difficult to sustain during long-term high--voltage cycling and lack a universal design principle, failing to address the root cause, that is, the intrinsic electronic structure of the solvent molecule itself [10,11]. Molecular engineering of solvents at the electronic level intrinsically enhances their high-voltage oxidation resistance [19,20]. This requires precise tuning of the molecule's electronic distribution (dipole moment) and coordination characteristics, which govern both bulk solvation structure and interfacial reaction pathways [21–23].

Herein, we proposed a molecular dipole modulation strategy to fundamentally redesign the ether solvent for high-voltage applications. By performing alkyl elongation and cyano-functionalization on the classic DME skeleton, we obtained 3-ethoxylated propionitrile (EPN). The alkoxy chain in the EPN molecule achieved an optimal balance between weakening the strong interaction between Li^+ and the cyano group (-C≡N) and maintaining essential solvation capabilities. The resulting solvation structure not only facilitated Li^+ de-solvation kinetics but also promoted the preferential decomposition of $DFOB^-$ anions and co-solvent fluoroethylene carbonate (FEC) at the electrode interface, constructing a stable interface rich in LiF and Li_3N, thereby simultaneously suppressing the Li dendrite growth and the side reactions on the cathode side. Consequently, the EPN-based electrolyte exhibited a widened electrochemical stability window up to 4.9 V. And full cells with $LiFePO_4$ and NCM712 using this well-designed electrolyte can run stably with a high CE. What's more, even matching with high loading cathode (24.78 mg cm^{-2}), the full cells can also demonstrate exceptional cycling stability. This work demonstrated that precise molecular-level design, targeting dipole moment and solvation moderation, can serve as a powerful paradigm to simultaneously stabilize the anode and cathode interfaces, paving a rational path toward practical high-voltage LMBs.

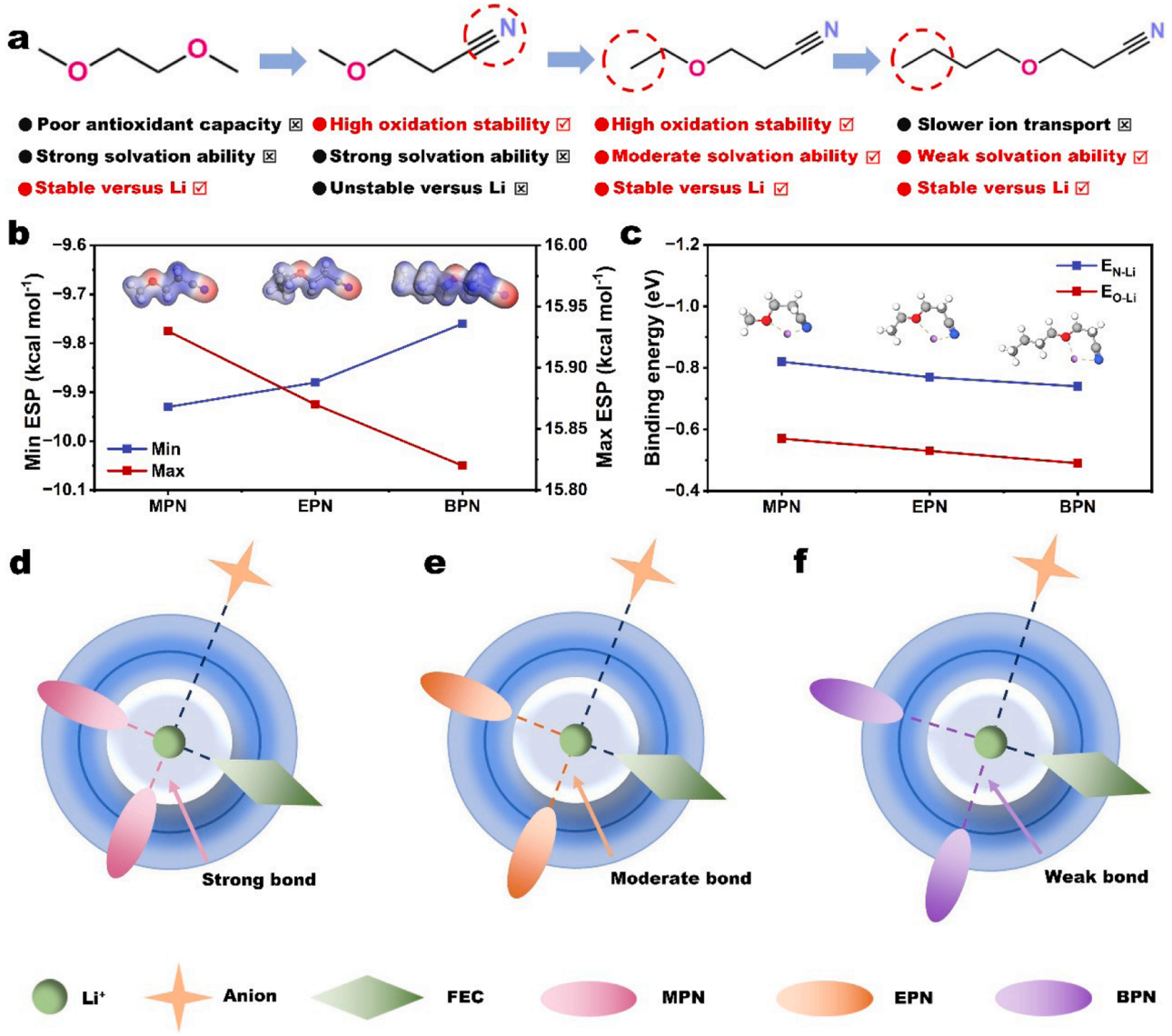

Fig. 1. Molecular design and dipole modulation. a) Solvent molecular design principles for high-voltage ether-based LMBs; b) ESP of MPN, EPN, and BPN; c) optimized structures and binding energies of Li^+-MPN, Li^+-EPN, and Li^+-BPN complexes; d-f) schematic illustration of electrolyte solvation structures dominated by d) strong (MPN), e) moderate (EPN), and f) weak (BPN) solvent coordination.

2. Results and discussion

2.1. Molecular design and the structure–property relationship

The molecular dipole modulation strategy was illustrated in Fig. 1a. Although traditional DME solvent exhibited excellent Li-metal compatibility and strong salt-dissociating ability, its narrow electrochemical window limited its application in high-voltage systems [11]. To overcome this limitation, replacing one methoxy group (–O–CH_3) with a highly polar cyano group (–C≡N) to obtain an asymmetric hybrid configuration, methoxypropionitrile (MPN). The cyano group not only displayed superior chemical stability over the ether linkage but also formed a strong and specific coordination with Li^+ [24,25]. Consequently, MPN demonstrated markedly enhanced oxidative stability compared to DME, though it also leaded to a higher de-solvation energy barrier for Li^+. However, the uncontrolled side reactions between the cyano group and Li metal would result in continuous consumption of both electrolyte and active Li, undermining long-term cycling [26].

Then, to reconcile high-voltage stability with interfacial compatibility, we further tuned the molecular structure by extending the alkoxy chain. Converting MPN to EPN moderately weakened the Li^+–N≡C interaction via steric effects. This "moderated coordination strength" promoted the formation of a stable interface and improved ion-transport kinetics. According to previous works, the term 'moderate solvation' refers to a coordination strength (quantified by Li^+–solvent binding energy) that is intermediate between strongly and weakly coordinating regimes [27–29]. This intermediate strength ensures sufficient ionic conductivity while maintaining a low de-solvation penalty at the electrode interface. In contrast, further extending the chain to butoxypropionitrile (BPN) introduced excessive steric hindrance, which impaired effective Li^+ coordination, thereby reducing solvation capability and slowing ion transport. This systematic structural variation allowed us to probe the subtle balance between coordination strength and bulk/interface properties. Long-term immersion tests were conducted to assess the chemical stability of MPN, EPN, and BPN toward the Li metal anode. As shown in **Figs. S1–2**, SEM and XPS analyses confirmed that the morphology and chemical state of the Li metal anodes remained unchanged after 24 h of immersion in the three solvents, indicating their high stability toward the Li metal anode.

To quantify these electronic and steric effects, we performed density functional theory (DFT) calculations [25,30]. As shown in Fig. 1b, the electrostatic potential (ESP) distributions revealed that as the alkoxy chain lengthened from MPN to EPN to BPN, the maximum ESP values gradually decreased while the minimum values increased, indicating that the electron-donating effect of additional C–C bonds subtly redistributed the electron density around the cyano nitrogen, thereby lowering its nucleophilicity and Li^+-coordinating ability, which was consistent with the designed dipole modulation.

The calculated binding energies of Li^+ to oxygen and nitrogen atoms further confirmed this conclusion, which was shown in Fig. 1c. For MPN molecule, minimal steric shielding allowed Li^+ to bind strongly to both sites ($E^+_{O\text{-}Li}$=−0.57 eV, $E^+_{N\text{-}Li}$=−0.82 eV). For EPN molecule, which added a –CH_2– unit compared to MPN, thus partially impeded close contact between Li^+ and the O/N atoms, leading to reduced binding energies ($E_{O\text{-}Li}{}^+$=−0.53 eV, $E^+_{N\text{-}Li}$=−0.77 eV). The electron-donating effect of the alkyl chain also attenuates the negative ESP on the cyano nitrogen, further weakening electrostatic attraction to Li^+. Here, the ethoxy extension in the EPN molecule precisely modulates the binding energy between the cyano group and Li^+, placing it within the ideal range of moderate strength. This avoids the de-solvation difficulty caused by overly strong binding while preventing insufficient ionic conductivity resulting from overly weak interaction. When the alkyl chain was further extended in BPN, the long and flexible butyl chain created substantial steric hindrance, severely hindering effective Li^+ coordination and resulting in the lowest binding energies.

Thus, the moderated binding energy of EPN molecule facilitated the formation of a thermodynamically stable yet kinetically agile solvation sheath. In contrast, excessively strong (MPN) or weak (BPN) binding disrupted this balance, respectively leading to high de-solvation penalties or inadequate ion-pair dissociation (Fig. 1d–f). Together, the molecular dipole modulation strategy established a clear molecular-level rationale for the superior performance of the EPN-based electrolyte, linking tailored dipole modulation to optimized solvation and interfacial behavior.

2.2. Solvation environment analysis

Building upon the molecular dipole modulation strategy, we next explore how the molecular structure governs the Li^+ solvation environment, which in turn dictates interfacial chemistry and battery performance. As shown in Fig. 2a–c and **Fig. S3**, molecular dynamics (MD) simulations of the different electrolyte systems revealed a clear trend: as the alkoxy chain lengthened from MPN to EPN to BPN, the solvent's coordination strength with Li^+ progressively weakened. What's more, in the EPN-based electrolyte (named as: EPF), a greater number of fluoroethylene carbonate (FEC) molecules entered the primary solvation sheath (Fig. 2b). This was the direct evidence of our molecular dipole modulation strategy: the ethoxy extension in EPN optimally moderated the binding energy of the cyano group with Li^+, creating a balanced coordination strength. This moderated solvation strength allowed EPN molecule to stably coordinate with Li^+ without monopolizing the solvation shell, thereby reserving coordination space and competitive opportunities for FEC molecules and creating a more dynamically balanced coordination environment. The increased presence of FEC favored the preferential formation of a LiF-rich, dense, and stable SEI film on the Li anode surface.

Concurrently, the MD simulations showed that as the alkyl chain lengthened, an increased number of $DFOB^-$ anions coordinated with Li^+. However, excessively long alkyl chains can reduce the overall polarity of the molecule and enhance its hydrophobicity, which may affect its compatibility with FEC components and its wettability toward electrodes (**Fig. S4**). This highlighted the importance of balance: the EPN molecule, with its tailored coordination capability, fostered synergistic cooperation among solvent, FEC, and $DFOB^-$. It constructed such a solvation sheath, which was sufficiently stable to support a stable solvation structure, yet sufficiently weak to allow for fast interfacial kinetics and stable interfacial chemistry. Furthermore, this optimized solvation structure was quantified by the coordination numbers. As shown in Fig. 2d and **Fig. S5**, in the MPN-based electrolyte (named as: MPF), the coordination number of each Li^+ for MPN molecules, $DFOB^-$ anions and FEC molecules was 2.23, 0.91 and 0.71, respectively. However, the EPF electrolyte systems exhibited significantly enhanced participation of $DFOB^-$ anions (1.06) and FEC molecules (0.77). As the alkyl chain lengthened, for the BPN-based electrolyte (named as: BPF) systems, the coordination number of $DFOB^-$ anions was enhanced to 1.27, whereas the coordination numbers of FEC molecules was 0.68. All results suggested that the moderate solvation capability can effectively balance interface stability and ion transport kinetics.

Moreover, the distance distributions between N/O atoms and Li^+ in different electrolyte systems was also analyzed, which was shown in Fig. 2e. Compared to MPF and BPF electrolyte systems, in the EPN-based electrolyte, the distances between the N/O atoms and Li^+ showed the smallest difference, indicating that the EPN molecule may simultaneously utilize its ether O atom and cyano N atom to form a more stable and compact semi-chelating structure with the Li^+. This balanced state of synergistic coordination was the structural origin of its moderated solvation capability. Further theoretical and spectroscopic analyses consolidated this conclusion. Frontier molecular orbital analysis revealed that although the LUMO energy levels of EPN molecule was similar to those of MPN and BPN molecules, the solvation structure in the EPF electrolyte possessed the lowest LUMO energy (Fig. 2f), which indicated that the $DFOB^-$ and FEC components in the EPF electrolyte

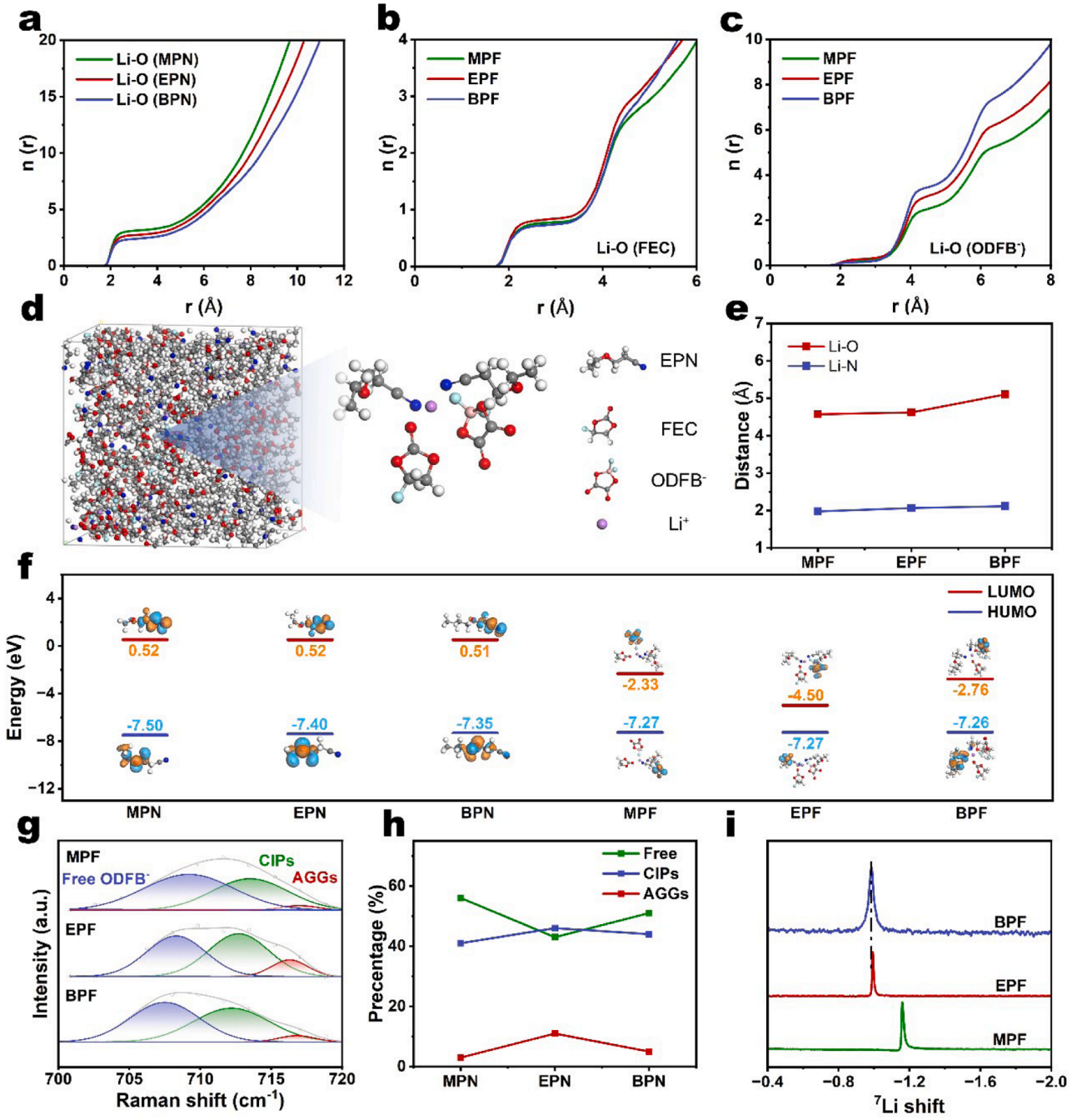

Fig. 2. Solvation structure and environment analysis. a–c) Coordination numbers of Li^+ with a) solvent molecules (MPN, EPN, BPN), b) FEC, and c) $DFOB^-$ anions derived from molecular dynamics simulations; d) snapshot from MD simulations of the EPF electrolyte (left) and a magnified view of a representative Li^+ solvation sheath (right); e) distribution of distances between Li^+ and the coordinating O/N atoms in MPN, EPN, and BPN; f) calculated HOMO and LUMO energy levels for the solvent molecules and Li^+-solvent-anion complexes in each electrolyte; g) Raman spectra of the MPF, EPF, and BPF electrolytes; h) deconvolution of the Raman spectra showing the relative proportions of free anions, contact ion pairs (CIPs), and aggregates (AGGs); i) ^7Li NMR spectra of the three electrolytes.

systems would be preferentially reduced at the Li metal anode surface, facilitating the early formation of a beneficial inorganic-rich SEI. At the same time, Raman spectroscopy confirmed a higher proportion of anion-involved aggregate (AGG) clusters in the EPF electrolyte systems, indirectly illustrating the formation of stable SEI film (Fig. 2g–h) [31,32]. The downfield shift in the ^7Li NMR spectra and the up-field shift in the ^{19}F NMR spectra confirm the varying solvation capabilities of the different electrolyte systems, which aligns well with the expectations of the molecular dipole modulation strategy (Fig. 2i **and Fig. S6)** [23]. Finally, solubility tests showed that as the alkoxy chain lengthened from MPN to EPN to BPN, the ability of the solvent to dissociate LiDFOB decreased, further confirming that steric hindrance from the alkoxy chain weakens solvent–Li^+ coordination **(Fig. S7)**.

2.3. *Interfacial kinetics and Li plating/stripping behavior*

The moderate solvation structure engineered in the EPF electrolyte translates directly into enhanced electrochemical stability and interfacial kinetics. As shown in Fig. 3a, Linear sweep voltammetry (LSV) demonstrated that the EPF electrolyte possessed the highest oxidative stability among the series. At the same time, we quantified the corresponding activation barriers of Li plating/stripping process, and Li||Li

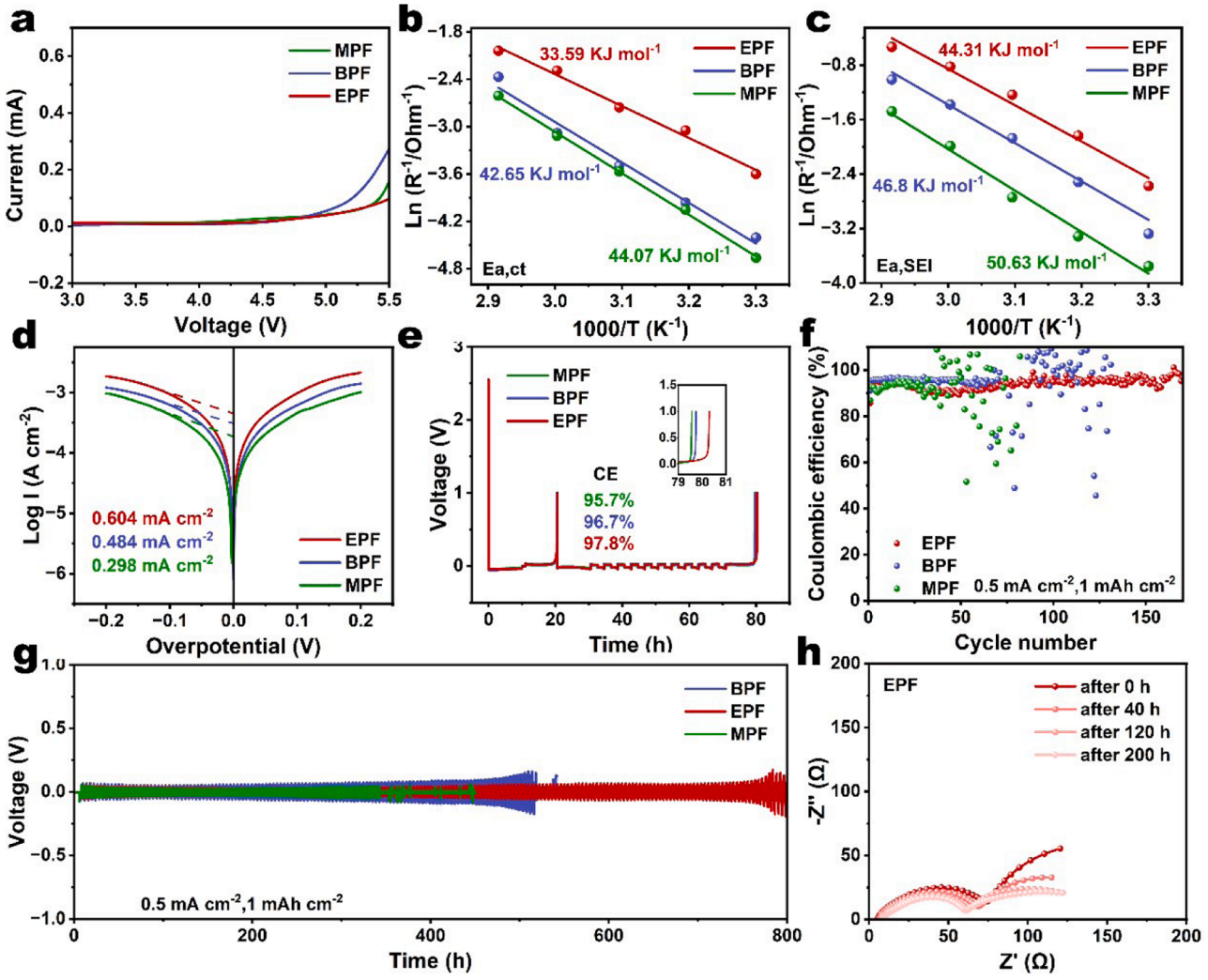

Fig. 3. Interfacial kinetics and Li plating/stripping behavior. a) LSV curves showing the electrochemical stability windows of the electrolytes; b, c) Fitted activation energies for b) Li^+ de-solvation and c) Li^+ diffusion through the SEI; d) Tafel plots obtained from Li||Li symmetric cells; e) average coulombic efficiency of Li|Cu cells; f) long-term cycling performance of Li|Cu cells at 0.5 mA cm^{-2} and 1.0 mAh cm^{-2}; g) voltage profiles of Li||Li symmetric cells at 0.5 mA cm^{-2}; h) Nyquist plots of Li||Li symmetric cells with the EPF electrolyte after different cycling periods.

symmetric cells were assembled and subjected to electrochemical impedance spectroscopy (EIS) tests at various temperatures. As shown in Fig. 3b–c and **Fig. S8**, after fitting with the Arrhenius equation, the EPF electrolyte exhibited the lowest activation energies for both Li^+ de-solvation (E_a, ct = 33.59 kJ mol^{-1}) and diffusion through the SEI (E_a, SEI = 44.31 kJ mol^{-1}). In contrast, the overly tight Li^+ coordination in MPF electrolyte resulted in the highest de-solvation barrier (44.07 kJ mol^{-1}), whereas the loose solvation structure in BPF electrolyte still leaded to a relatively high barrier (42.65 kJ mol^{-1}) due to the involvement of more anions, highlighting the advantage of moderate solvation structure in kinetics [33]. Meanwhile, the EIS and desolvation energy fitting results at low temperatures show that the EPF electrolyte has the lowest desolvation energy barrier, demonstrating the adaptability of the molecular dipole regulation strategy under low-temperature conditions **(Fig. S9)**.

This kinetic advantage was further reflected in the interfacial charge-transfer process. As shown in Fig. 3d, Tafel analysis revealed that the EPF electrolyte achieved the highest exchange current density (0.604 mA cm^{-2}), significantly exceeding those of BPF electrolyte (0.484 mA cm^{-2}) and MPF electrolyte (0.298 mA cm^{-2}). This indicated that the moderate solvation structure in EPF electrolyte enabled faster intrinsic reaction kinetics for Li plating/stripping process.

The moderate solvation structure was beneficial for half-cell cycling performance. As shown in Fig. 3e, Li||Cu cells employing the EPF electrolyte achieved a high average Coulombic efficiency (CE) of 97.8 %, indicative of excellent interfacial reversibility. The CV test results of the Li||Cu half cells with different electrolyte systems showed the good chemical compatibility of EPN and BPN toward the Li metal anode (**Fig. S10**). Moreover, in long-term cycling at 0.5 mA cm^{-2} and 1.0 mAh cm^{-2}, the half cells using the EPF electrolyte still maintained a stable CE of 98.4 % over 170 cycles, while the cells cycling in the BPF and MPF electrolyte systems exhibited significant fluctuations after only 75 and 30 cycles, respectively (Fig. 3f), which once again proved that the advantage of moderate solvation structure in stabilizing interfaces and electrochemical cycling process.

Similarly, Li||Li symmetric cells with EPF electrolyte also demonstrated exceptional cycling stability for over 800 h with low and stable overpotentials, benefiting from the optimized solvation structure and low activation barriers (Fig. 3g). In contrast, the symmetric cells cycling in the BPF and MPF electrolyte systems exhibited obvious overpotential fluctuations and quickly failed, corresponding to severe interface side reactions and unstable SEI layer. Meanwhile, the EIS results after different cycles further confirmed that the symmetric cells with EPF electrolyte exhibited the lowest and most stable interfacial impedance, affirming the simultaneous achievement of fast kinetics and high SEI stability (Fig. 3h and **Fig. S11**) [34].

The interfacial stability was also analyzed by SEM after Li deposition. As shown in Fig. 4a, at a current density of 1.0 mA cm^{-2}, in-situ optical microscopy showed that the Li deposition in the MPF electrolyte was mossy dendrites, whereas both EPF and BPF electrolyte enabled denser and more uniform Li deposition. At the same time, the SEM images showed that the Li metal anode cycled in EPF electrolyte remained homogeneous and compact over extended cycling, with no observable dendrites (Fig. 4b–d and **Fig. S12**). The chemical composition of the SEI, characterized by X-ray photoelectron spectroscopy (XPS), provides the underlying reason for the interfacial stability, which was shown in Fig. 4e–g and **Figs. S13–14**. In the F1s spectra, the peak at 684.8 eV corresponds to the formation of LiF. A higher LiF content was observed on the Li metal anode surface when cycling in the EPF electrolyte, which can enhance the mechanical strength, chemical stability of the SEI [25, 30]. Furthermore, B–F bonds from intermediate products of $ODFB^-$ decomposition provided certain flexibility to the SEI and a higher content of Li_3N, improving Li^+ conductivity within the interphase [24, 35–38]. This uniquely robust SEI layer, fostered by the moderate solvation structure in the EPF electrolyte, is fundamental to the high interface kinetics and long-term cycling stability.

2.4. Electrochemical performance and application

The practical application of the molecular dipole modulation strategy was evaluated in full cells paired with both $LiFePO_4$ (LFP) and high-voltage NCM712 cathodes. Firstly, the long-term cycling performance of Li||LFP cells at 1.0 C revealed the superior stability of the EPF electrolyte (Fig. 5a). It retained 80 % of its initial capacity after 540 cycles with an average Coulombic efficiency (CE) of 99.94 %, significantly outperforming cells with MPF electrolyte (35.8 % retention after 350 cycles) and BPF electrolyte (61.4 % retention after 330 cycles). At the same time, the charge/discharge curves at different cycles indicated severe structural degradation and capacity decay when using MPF and BPF electrolyte compared to those with EPF electrolyte (**Fig. S15**).

Beyond cycling stability, the EPF electrolyte also demonstrated outstanding rate performance. As shown in Fig. 5b and **Fig. S16**, the full cells with EPF electrolyte delivered discharge capacities of 163.06, 155.41, 149.32, 140.87, and 125.63 mAh g^{-1} at 0.5 C, 1.0 C, 2.0 C, 3.0 C, and 5.0 C, respectively. This outstanding kinetics stems from the moderate solvation structure, which balances efficient Li^+ coordination with fast desolvation and interfacial stability. In contrast, the full cells

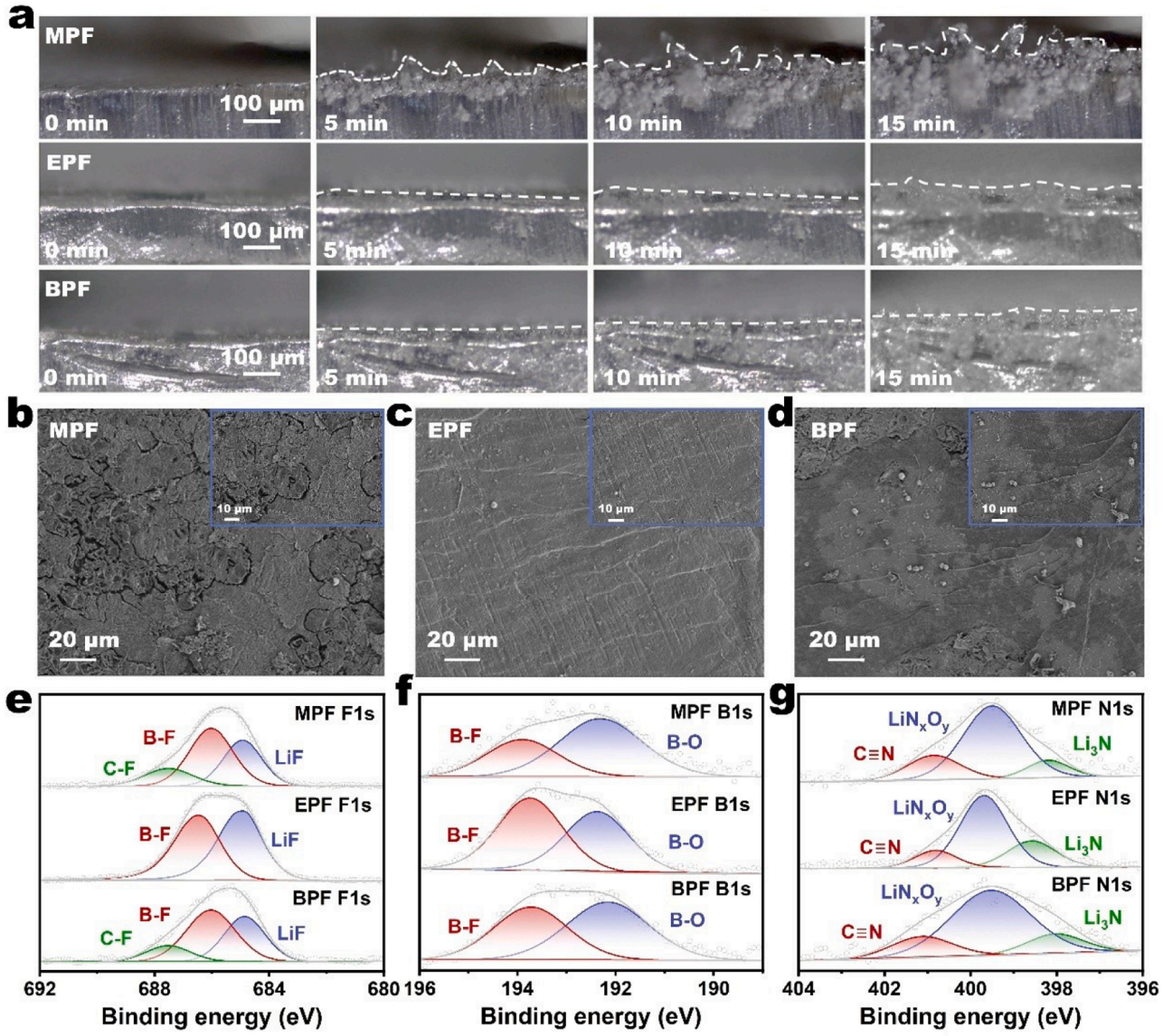

Fig. 4. Li deposition morphology and post analysis. a) In-situ optical microscopy of Li deposition in different electrolytes; b–d) SEM images of Li metal anodes after 50 cycles in b) MPF, c) EPF, and d) BPF electrolytes; e–g) XPS spectra of cycled Li electrodes, e) F 1 s, f) B 1 s, and g) N 1 s.

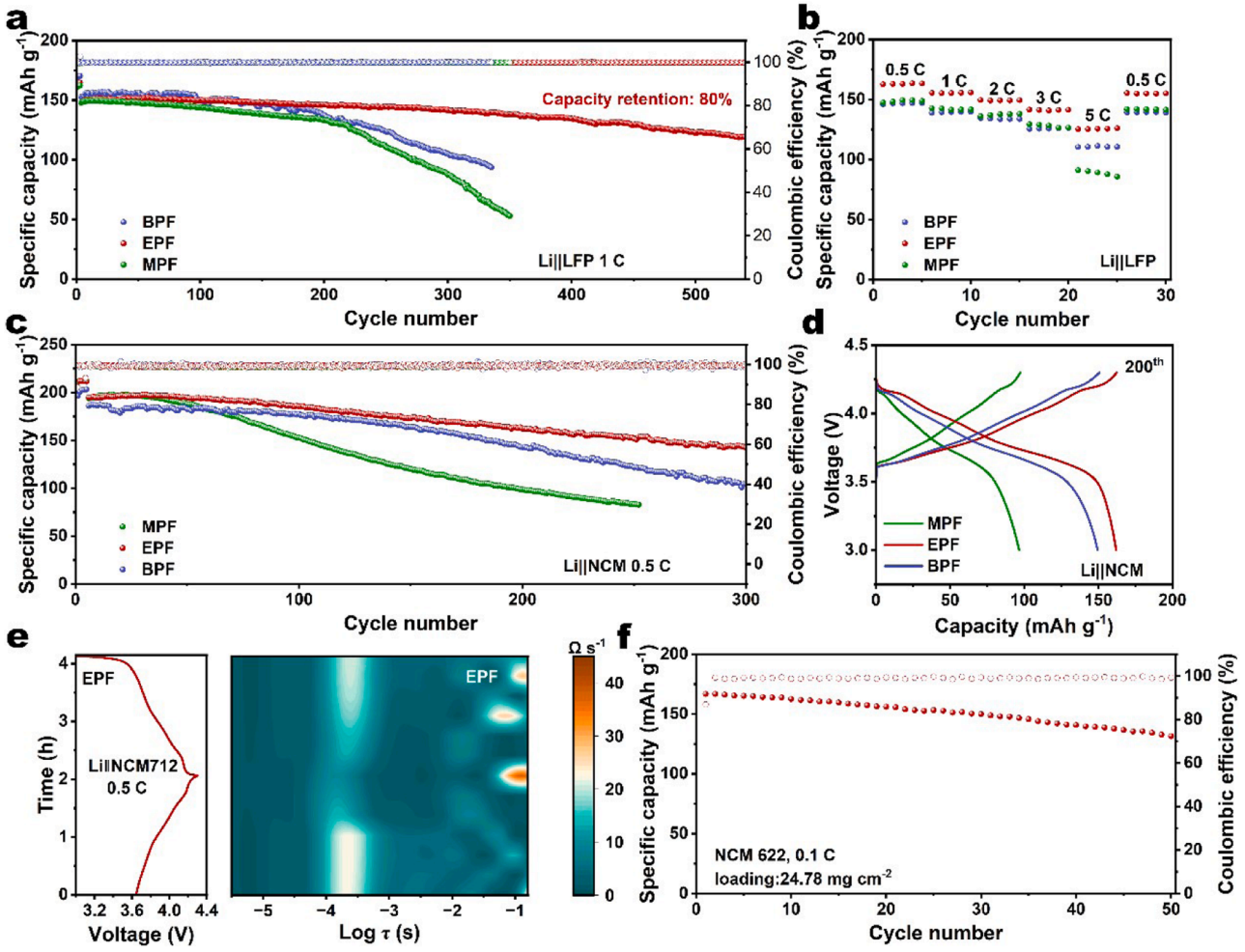

Fig. 5. Full cells and application. a) Long-term cycling performance of Li||$LiFePO_4$ cells at 1.0 C; b) rate capability of Li||$LiFePO_4$ cells; c) cycling stability of Li||NCM712 cells at 0.5 C; d) selected charge–discharge voltage profiles of Li||NCM712 cells during cycling; e) DRT analysis derived from Li||NCM712 cells with the EPF electrolyte; f) Cycling performance of a high-loading full cell (24.78 mg cm^{-2}) with EPF electrolyte.

using the MPF and BPF electrolyte systems exhibited markedly lower capacities at high rates due to their respective kinetic limitations.

The advantage of EPF electrolyte becomes even more critical under high-voltage conditions. When matching with high-voltage NCM712 cathode, the full cells using EPF electrolyte can also achieve a high capacity retention of 73.1 % after 300 cycles, far exceeding the BPF electrolyte (56 %) and MPF electrolyte, which suffered rapid failure within 60 cycles (Fig. 5c–d), corresponding to severe oxidative decomposition of electrolyte and high Li^+ desolvation barrier at high voltage. To probe the interfacial evolution, In-situ electrochemical impedance spectroscopy combined with distribution of relaxation time (DRT) analysis was performed on Li||NCM712 cells, which was shown in Fig. 5e and **Fig. S17** [39]. The cells using the EPF electrolyte displayed more pronounced relaxation behavior, indicating the formation of a more stable SEI during cycling, which facilitated rapid Li^+ transport. Furthermore, the full cells assembled with high-loading cathodes (24.78 mg cm^{-2}) were tested to validate the practical applicability of EPF electrolyte, which was shown in Fig. 5f. And the cells can also maintain stable cycling over 50 cycles, demonstrating its potential for high-energy-density applications.

Post-cycling XPS analysis of the NCM712 cathodes after cycling in the EPF electrolyte provides chemical insight into the interface stability. As shown in Fig. 6a–d and **Fig. S18**, in the C 1 s spectra, the peaks corresponding to organic products such as C–O and $C=O$ were weaker and no detectable C–F, indicating an inorganic-dominated cathode electrolyte interphase (CEI) [25]. Meanwhile, the F 1 s spectra confirmed a substantially higher LiF content in the EPF-derived CEI, which reinforced interfacial mechanical and chemical stability [30]. Additionally, B 1 s and N 1 s spectra showed the highest concentrations of B–F bonds and Li_3N in the EPF-derived CEI, where the former originated from the decomposition of $ODFB^-$ and the latter from EPN decomposition, indicating improved Li^+ transport efficiency and interface stability [36–38].

FIB-SEM was employed to examine the structural integrity of cathodes after cycling. As shown in Fig. 6e–g, the cathode cycled with the MPF electrolyte displayed severe particle cracking, symptomatic of mechanical degradation and extensive side reactions. The BPF electrolyte, while less destructive, also induced noticeable cracks. In contrast, the cathode cycled in the EPF electrolyte exhibited a pristine and intact cross-section, demonstrating the superior protection afforded by its stable CEI. The cycled NCM712 cathode was further characterized by TEM. As shown in Fig. 6h–j, compared to the thicker and non-uniform CEI observed in MPF and BPF, the CEI formed in EPF was thinner and more homogeneous, further confirming that EPF facilitated the formation of a more stable and uniform CEI.

Collectively, the molecularly tailored EPF electrolyte establishes a moderate solvation environment that avoids excessive Li^+ binding, which promotes the formation of a stable interphase, that is, a stable SEI on the anode and a stable CEI on the cathode (Fig. 6k), thereby ensuring the high-rate capability and long-term cycling stability of high-voltage LMBs.

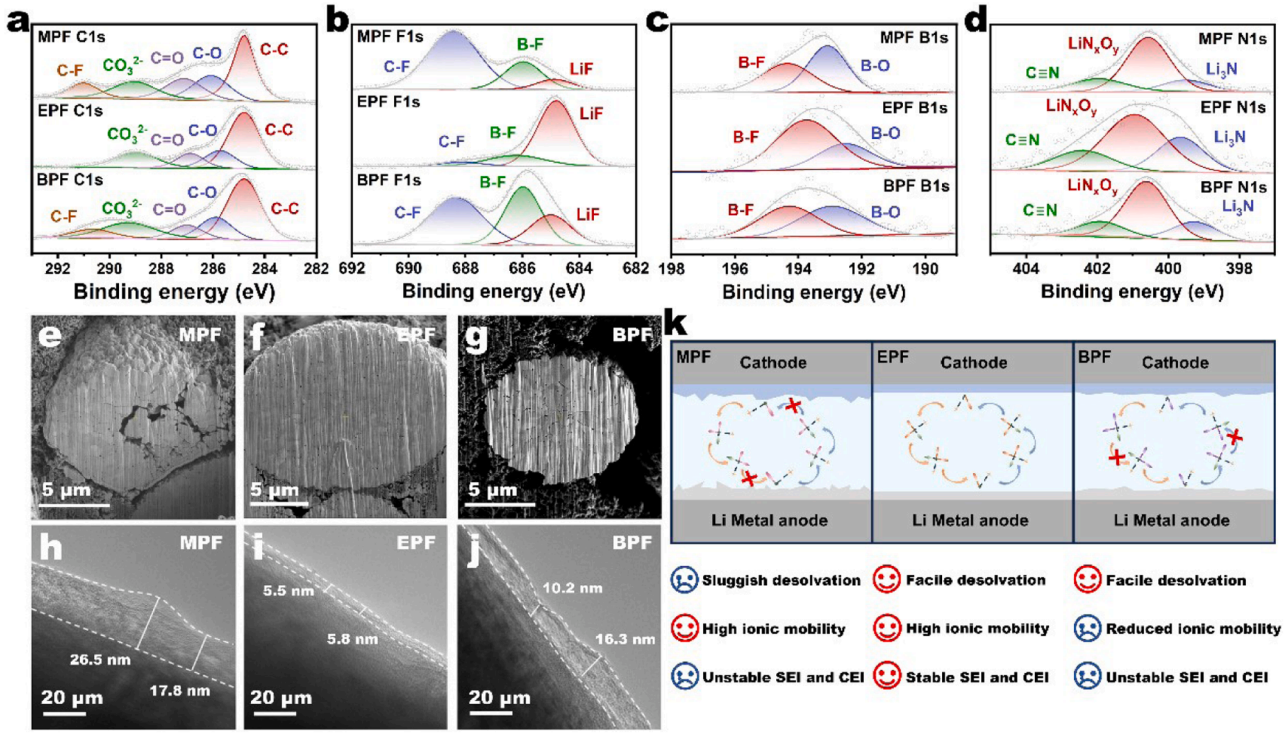

Fig. 6. Post analysis of the cycled NCM712 electrode. a–d) XPS spectra of the NCM712 cathodes after cycling, a) C 1 s, b) F 1 s, c) B 1 s, and d) N 1 s; FIB-SEM characterization of cross-section morphologies of cathode particles cycled in e) MPF, f) EPF, and g) BPF electrolytes after 50 cycles; TEM images of NCM712 cathodes cycled with h) MPF, i) EPF and j) BPF after 50 cycles; k) schematic illustrating Li^+ migration and de-solvation mechanisms in electrolytes with different solvation structures.

3. Conclusion

In summary, we have demonstrated that the molecular dipole modulation strategy offers an effective pathway to simultaneously address solvation structure and interfacial stability in ether-based electrolytes for high-voltage LMBs. By incorporating an extended ethoxy chain and a cyano group into the classical DME skeleton, the designed EPN solvent achieves a moderated solvation strength. This tailored coordination environment reduces the Li^+ de-solvation barrier and promotes the formation of stable interface, thereby effectively suppressing side reactions and Li dendrite growth. Benefiting from this rational design, the EPN-based electrolyte enables remarkable full-cell performance. Li||NCM712 cells achieve 73.1 % capacity retention over 300 cycles at 0.5 C. Even under practical conditions with a high-loading NCM cathode (24.78 mg cm^{-2}), stable cycling can also be achieved for 50 cycles. These results highlight the critical role of balanced solvation in achieving high-voltage compatibility and long-term cycling stability. This work provides a forward-looking strategy for developing advanced electrolytes, paving the way toward high-energy-density LMBs capable of stable operation at high voltages.

4. Experimental section/methods

Full details of all experiments are provided in Supporting Information.

CRediT authorship contribution statement

Jiping Ma: Writing – original draft, Data curation. **Bo Zhang:** Formal analysis. **Yang Gao:** Investigation. **Lifeng Hou:** Investigation. **Yinghui Wei:** Formal analysis, Conceptualization. **Shi Wang:** Data curation. **Zhong Jin:** Methodology, Investigation. **Qian Wang:** Writing – review & editing, Resources, Formal analysis, Data curation, Conceptualization.

Declaration of competing interest

The authors declare that they have no known competing financial interests or personal relationships that could have appeared to influence the work reported in this paper.

Acknowledgements

This work was supported by the National Natural Science Foundation of China (No. 22402146, 22572140, U24A6002), the Beijing Natural Science Foundation Xiaomi innovation joint Foundation (L223011), Young Elite Scientists Sponsorship Program by CAST (2022QNRC001), Shanxi energy internet research institute (SXEI2023A004), Open Research Fund of Guangdong Advanced Carbon Materials Co., Ltd. (Kargen-2024B0905), the special fund for Science and Technology Innovation Teams of Shanxi Province (202204051001004).

Supplementary materials

Supplementary material associated with this article can be found, in the online version, at doi:10.1016/j.ensm.2026.105063.

Data availability

Data will be made available on request.

References

[1] B. Liu, J.G. Zhang, W. Xu, Advancing lithium metal batteries, Joule 2 (2018) 833–845, https://doi.org/10.1016/j.joule.2018.03.008.
[2] X. Xu, J. Chen, Z.M. Zhou, X.S. Zhang, X.H. Zeng, Y. Wan, S.H. Zhou, X.Q. Wu, X. Chen, X.Z. Zhou, J.Z. Wang, S.L. Chou, L. Li, Eutectic electrolytes for high-performance lithium/sodium metal batteries, Adv. Energy Mater. 15 (2025) 2503001, https://doi.org/10.1002/aenm.202503001.

[3] Q. Wang, T.T. Lu, Y. Liu, J. Dai, L.X. Guan, L.F. Hou, H.Y. Du, H. Wei, X.D. Liu, X. Q. Han, Z.X. Ye, D. Zhang, Y.H. Wei, H.H. Zhou, Li+ migration and transformation at the interface: a review for stable Li metal anode, Energy Storage Mater. 55 (2023) 782–807, https://doi.org/10.1016/j.ensm.2022.12.043.
[4] S. Liu, B. Wu, X. Bai, J.H. Zhang, X.Y. Chang, L.F. Hou, H. Huang, Y.H. Wei, S. Wang, Z. Jin, Q. Wang, A solvent-induced solid polymer electrolyte with controllable polymerization for low-temperature lithium metal batteries, Nano Lett. 25 (2025) 5241–5249, https://doi.org/10.1021/acs.nanolett.4c06471.
[5] X. He, D. Bresser, S. Passerini, F. Baakes, U. Krewer, J. Lopez, C.T. Mallia, Y. Shao-Horn, I. Cekic-Laskovic, S. Wiemers-Meyer, F.A. Soto, V. Ponce, J.M. Seminario, P. B. Balbuena, H. Jia, W. Xu, Y.B. Xu, C.M. Wang, B. Horstmann, R. Amine, C.C. Su, J.Y. Shi, K. Amine, M. Winter, A. Latz, R. Kostecki, The passivity of lithium electrodes in liquid electrolytes for secondary batteries, Nat. Rev. Mater. 6 (2021) 1036–1052, https://doi.org/10.1038/s41578-021-00345-5.
[6] Q. Wang, T.T. Lu, Y.B. Xiao, J.Y. Wu, L.X. Guan, L.F. Hou, H.Y. Du, H. Wei, X. D. Liu, C.K. Yang, Y.H. Wei, H.H. Zhou, Y. Yu, Leap of Li metal anodes from coin cells to pouch cells: challenges and progress, Electrochem. Energy Rev. 6 (2023) 22, https://doi.org/10.1007/s41918-023-00185-7.
[7] F. Hai, Y.Y. Ban, W.C. Xue, Y.X. Yang, W.T. Yan, W.B. Hua, W. Tang, M.T. Li, Rational design of ether-based localized weak solvation liquid electrolyte for practical lithium metal batteries, Adv. Funct. Mater. (2025) e14536, https://doi.org/10.1002/adfm.202514536.
[8] C.C. Su, J.Y. Shi, R. Amine, M.N. He, S.B. Son, J.C. Guo, M. Jiang, K. Amine, Terminally fluorinated glycol ether electrolyte for lithium metal batteries, Nano Energy. 110 (2023) 108335, https://doi.org/10.1016/j.nanoen.2023.108335.
[9] J.M. Zhang, Q.P. Li, Y.P. Zeng, Z. Tang, D. Sun, D. Huang, Z.G. Peng, Y.G. Tang, H. Y. Wang, Non-flammable ultralow concentration mixed ether electrolyte for advanced lithium metal batteries, Energy Storage Mater. 51 (2022) 660–670, https://doi.org/10.1016/j.ensm.2022.07.014.
[10] J.W. Chen, D.M. Zhang, L. Zhu, M.Z. Liu, T.L. Zheng, J. Xu, J. Li, F. Wang, Y. G. Wang, X.L. Dong, Y.Y. Xia, Hybridizing carbonate and ether at molecular scales for high-energy and high-safety lithium metal batteries, Nat. Commun. 15 (2024) 3217, https://doi.org/10.1038/s41467-024-47448-5.
[11] I. Choi, Y.L. Chen, A. Shah, J. Florian, C. Serrao, J. Holoubek, H. Lyu, E. Zhang, J. H. Lee, Y.J. Lin, S.C. Kim, H. Park, P. Zhang, J.Y. Lee, J. Qin, Y. Cui, Z.A. Bao, Asymmetric ether solvents for high-rate lithium metal batteries, Nat. Energy. 10 (2025) 365–379, https://doi.org/10.1038/s41560-025-01716-w.
[12] S. Li, H.L. Xie, P. Kumar, Y.H. Chen, J. Wang, A.K. Huang, W. Wahyudi, H. Zhu, J. Yin, Q. Li, Z. Ma, J. Ming, Ether-oxygen groups modified carboxylic ester enabling high-voltage lithium metal batteries, Angew. Chem. Int. Ed. 64 (2025), https://doi.org/10.1002/anie.202504490 e202504490.
[13] Q. Wang, S. Wang, T.T. Lu, L.X. Guan, L.F. Hou, H.Y. Du, H. Wei, X.D. Liu, Y. H. Wei, H.H. Zhou, Ultrathin solid polymer electrolyte design for high-performance Li metal batteries: a perspective of synthetic chemistry, Adv. Sci. 10 (2023) 2205233, https://doi.org/10.1002/advs.202205233.
[14] T. Li, Y. Li, Y.L. Sun, Z.F. Qian, R.H. Wang, New insights on the good compatibility of ether-based localized high-concentration electrolyte with lithium metal, ACS Mater. Lett. 3 (2021) 838–844, https://doi.org/10.1021/acsmaterialslett.1c00276.
[15] S.S. Lin, H.M. Hua, Z.S. Li, J.B. Zhao, Functional localized high-concentration ether-based electrolyte for stabilizing high-voltage lithium-metal battery, ACS Appl. Mater. Interfaces. 12 (2020) 33710–33718, https://doi.org/10.1021/acsami.0c07904.
[16] F.L. Qiu, X. Li, H. Deng, D. Wang, X.W. Mu, P. He, H.S. Zhou, A concentrated ternary-salts electrolyte for high reversible Li metal battery with slight excess Li, Adv. Energy Mater. 9 (2019) 1803372, https://doi.org/10.1002/aenm.201803372.
[17] X.D. Ren, L.F. Zou, S.H. Jiao, D.H. Mei, M.H. Engelhard, Q.Y. Li, H.Y. Lee, C.J. Niu, B.D. Adams, C.M. Wang, J. Liu, J.G. Zhang, W. Xu, High-concentration ether electrolytes for stable High-voltage lithium metal batteries, ACS Energy Lett. 4 (2019) 896–902, https://doi.org/10.1021/acsenergylett.9b00381.
[18] S. Shen, D.D. Chai, X. Li, Y.Z. Fu, The synergistic effect of anion: design of stable ether electrolytes for Li metal batteries beyond 4.6 V, Adv. Funct. Mater. 35 (2025) 2424072, https://doi.org/10.1002/adfm.202424072.
[19] G.Z. Zhang, T. Zhang, Y.Q. Liu, Q.R. Wang, R.L. He, P.X. Li, Y.M. Cui, Z.B. Liu, C. Y. Wang, Y.H. Deng, J. Chang, J. Lu, Molecular design of asymmetric difluorinated ether electrolytes for stable operation of high-voltage lithium metal batteries, Angew. Chem. Int. Ed. 64 (2025), https://doi.org/10.1002/anie.202506056 e202506056.
[20] G.Z. Zhang, T. Zhang, Z. Zhang, R.L. He, Q.R. Wang, S.S. Chi, Y.M. Cui, M.D. Gu, Z. B. Liu, J. Chang, C.Y. Wang, K. Xu, Y.H. Deng, High-energy and fast-charging lithium metal batteries enabled by tuning Li+-solvation via electron-withdrawing and lithiophobicity functionality, Nat Commun. 16 (2025) 4722, https://doi.org/10.1038/s41467-025-59967-w.
[21] Y.L. Chen, Z. Yu, P. Rudnicki, H.X. Gong, Z.J. Huang, S.C. Kim, J.C. Lai, X. Kong, J. Qin, Y. Cui, Z.N. Bao, Steric effect tuned ion solvation enabling stable cycling of high-voltage lithium metal battery, J. Am. Chem. Soc. 143 (2021) 18703–18713, https://doi.org/10.1021/jacs.1c09006.
[22] J.L. Liang, S.Y. Sun, N. Yao, Z. Zheng, Q.K. Zhang, B.Q. Li, X.Q. Zhang, J.Q. Huang, Regulating the electrolyte solvation structure by weakening the solvating power of solvents for stable lithium metal batteries, Sci. China Chem. 66 (2023) 3620–3627, https://doi.org/10.1007/s11426-023-1730-x.
[23] J.H. Chen, H.C. Lu, X.R. Kong, J. Liu, J.Q. Liu, J. Yang, Y. Nuli, J.L. Wang, Interphase engineering via solvent molecule chemistry for stable lithium metal batteries, Angew. Chem. Int. Ed. 63 (2024), https://doi.org/10.1002/anie.202317923 e20231792.
[24] S. Wu, X.Y. Liu, Z.M. Hao, X.W. Sun, J.Z. Hou, L. Shang, L.Y. Wang, K. Zhang, H. X. Li, Z.H. Yan, J. Chen, Uncovering the crucial role of chelating structures in cyano-alkyl-phosphate electrolytes for high-voltage lithium metal batteries, J. Am. Chem. Soc. 146 (2024) 28770–28782, https://doi.org/10.1021/jacs.4c07739.
[25] M.L. Mao, L. Gong, X.B. Wang, Q.Y. Wang, G.Q. Zhang, H.X. Wang, W. Xie, L. M. Suo, C.L. Wang, Electrolyte design combining fluoro- with cyano- substitution solvents for anode- free Li metal batteries, Proc. Natl. Acad. Sci. U.S.A. 121 (2024) e2316212121, https://doi.org/10.1073/pnas.2316212121.
[26] T.Q. Yang, J.T. Lou, L.Y. Hu, Q. Liu, Z.Y. Huang, Q.R. Zhou, H.Y. Zhang, W.L. Song, H. Huang, Y. Wang, X.Y. Tao, Y. Xia, W.K. Zhang, J. Zhang, In situ construction of LiF/Li3N/LixGa hybrid SEI to boost long-lifespan succinonitrile-based solid-State lithium metal batteries, Adv. Funct. Mater. 35 (2025) 2423719, https://doi.org/10.1002/adfm.202423719.
[27] M.C. Li, Y.Q. Chen, S.R. Wu, W. Wang, J. Zhou, Q.F. Fu, P.T. Xiao, J.L. Liu, Tuning solvation structure via inductive and steric hindrance effects for high-voltage LiCoO2 batteries, Angew. Chem. Int. Ed. 64 (2025) e202514299, https://doi.org/10.1002/anie.202514299.
[28] Y. Wei, H. Wang, X. Lin, T.Y. Wang, Y.M. Cui, Y. Huang, J.Y. Yang, T.H. Liu, Y. Ren, X.L. Fan, H.H. Xu, Y.H. Huang, Moderate solvation structures of lithium ions for high-voltage lithium metal batteries at-40 °C, Energy Environ. Sci. 18 (2025) 786–798, https://doi.org/10.1039/d4ee03192j.
[29] C.F. Zhang, J.Y. Peng, S.J. Cheng, J. Xie, Electrolyte chemistry design via mediumly solvating structure for high-voltage and low-temperature aqueous batteries, Adv. Funct. Mater. 36 (2025), https://doi.org/10.1002/adfm.202516909 e16909.
[30] H.P. Zhu, Q.F. Zhang, K.F. Wang, G. Zhou, P. Huang, Z. Chen, L.B. Chen, C. X. Zhang, W.F. Wei, Minimizing solvent-coordination in ether electrolytes for lithium metal batteries under extreme operating conditions, Adv. Mater. 37 (2025) 2505892, https://doi.org/10.1002/adma.202505892.
[31] K. Ding, C. Xu, Z.H. Peng, X. Long, J.K. Shi, Z.L. Li, Y.P. Zhang, J.W. Lai, L.Y. Chen, Y.P. Cai, Q.F. Zheng, Tuning the solvent alkyl chain to tailor electrolyte solvation for stable Li-metal batteries, ACS Appl. Mater. Interfaces. 14 (2022) 44470–44478, https://doi.org/10.1021/acsami.2c13517.
[32] T.H. Xu, T.L. Zheng, Z.Z. Ru, J.H. Song, M.R. Gu, Y. Yue, Y.Y. Xiao, S. Amzil, J. Gao, P. Müller-Buschbaum, K. Wang, H.B. Zhao, Y.J. Cheng, Y.G. Xia, Ether-based electrolyte for high-temperature and high-voltage lithium metal batteries, Adv. Funct. Mater. 34 (2024) 2313319, https://doi.org/10.1002/adfm.202313319.
[33] K. Xu, A. von Cresce, U. Lee, Differentiating contributions to "ion transfer" barrier from interphasial resistance and Li+ desolvation at electrolyte/graphite interface, Langmuir 26 (2010) 11538–11543, https://doi.org/10.1021/la1009994.
[34] J.Y. Wu, S.P. Zhang, C.K. Yang, X.X. Zhang, M.Y. Zhou, W. Liu, H.H. Zhou, Rational design of hierarchically-solvating electrolytes enabling highly stable lithium metal batteries with high-nickel cathodes, Energy Storage Mater. 63 (2023) 103043, https://doi.org/10.1016/j.ensm.2023.103043.
[35] X. Li, Y. Bai, J.X. Jing, T. Ren, Z.H. Wang, J.M. Ma, K.N. Sun, Cyano-functionalized hybrid electrode-electrolyte interphases enabled by Cyano-substituted tetrafluorobenzene derivatives additives for high-voltage lithium metal batteries, Adv. Funct. Mater. 35 (2025) 2421329, https://doi.org/10.1002/adfm.202421329.
[36] Z.M. Hao, X.X. Liu, Y. Li, J.D. Liu, H.D. Li, L.L. Wang, G.J. Yang, J.M. Ma, Additive-mediated anion sieving coordination strategy for long-lifespan lithium metal pouch cell with energy density over 540 wh kg-1, Adv. Energy Mater. 15 (2025) 2502242, https://doi.org/10.1002/aenm.202502242.
[37] Q. Liu, Y.K. Sun, M.Y. Li, Z.X. Xu, Y. Nuli, J.L. Wang, J. Yang, Branched ether-driven electrolyte engineering for resilient inorganic-polymeric interface on micro-silicon anodes in high-energy Li-ion batteries, Adv. Funct. Mater. (2025), https://doi.org/10.1002/adfm.202513046 e13046.
[38] L. Wang, Y.P. Qu, C. Su, R.Y. Li, D.M. Liu, W.Y. Jiang, X. Jin, M.F. Pei, X.G. Jian, F. Y. Hu, Interfacial engineering of Li anode and Ni-rich cathode via anion-regulated SEI/CEI layers in flame-retardant nanofiber-reinforced polymer electrolyte for lithium metal batteries, Adv. Energy Mater. 15 (2025) 2501185, https://doi.org/10.1002/aenm.202501185.
[39] B.R. Yang, Y.K. Wang, R.X. Zheng, W. Yang, Y.J. Li, T. Li, K. Li, A.J. Hu, J.P. Long, S.J. Ding, Conformational engineering of solvent molecules for high-voltage and fast-charging lithium metal batteries, Angew. Chem. Int. Ed. 64 (2025), https://doi.org/10.1002/anie.202508486 e202508486.